Nanoscale Advances

PAPER

View Article Online
View Journal | View Issue

Cite this: *Nanoscale Adv.*, 2022, **4**, 3182

Multivalent stimulation of β_1-, but not β_2-receptors by adrenaline functionalised gold nanoparticles†

Annabelle Mattern,[a] Rebecca Claßen,[*b] Annemarie Wolf,[c] Ervice Pouokam,[b] Klaus-Dieter Schlüter,[c] Mathias S. Wickleder[a] and Martin Diener[b]

In this study, we present a strategy for the synthesis of catecholamine functionalised gold nanoparticles and investigated their multivalent interactions with adrenergic receptors in different biological systems. The catecholamines adrenaline and noradrenaline represent key examples of adrenergic agonists. We used gold nanoparticles as carriers and functionalised them on their surface with a variety of these neurotransmitter molecules. For this purpose, we synthesised each ligand separately using mercaptoundecanoic acid as a bifunctional linking unit and adrenaline (or noradrenaline) as a biogenic amine. This ligand was then immobilised onto the surface of presynthesised spherical monodispersive gold nanoparticles in a ligand exchange reaction. After detailed analytical characterisations, the functionalised gold nanoparticles were investigated for their interactions with adrenergic receptors in intestinal, cardiac and respiratory tissues. Whereas the contractility of respiratory smooth muscle cells (regulated by β_2-receptors) was not influenced, (nor)adrenaline functionalised nanoparticles administered in nanomolar concentrations induced epithelial K^+ secretion (mediated *via* different β-receptors) and increased contractility of isolated rat cardiomyocytes (mediated by β_1-receptors). The present results suggest differences in the accessibility of adrenergic agonists bound to gold nanoparticles to the binding pockets of different β-receptor subtypes.

Received 20th March 2022
Accepted 25th June 2022

DOI: 10.1039/d2na00171c

rsc.li/nanoscale-advances

Introduction

Nanoparticles (NPs) can have a large variety of possible applications reaching from dyes[1] and catalysts in industry,[2] over packing applications[3] or sensors in the food industry,[4] to tumour markers[5] or targeted pharmacotherapy in medicine.[6] Physicochemical properties of NPs differ from their bulk material and thus they are of high interest due to their unique magnetic,[7] optical[8] or mechanical properties.[9]

Gold nanoparticles (Au NPs) represent an exceptionally well-known example. Due to their unique plasmon resonance, Au NPs deviate significantly in their wine-red colour from the metallic shine of the bulk material. A variety of potential applications exists for Au NPs. In 1989, Haruta *et al.*[10] described the oxidation of CO catalysed by Au NPs; thus these nanomaterials have been widely studied as catalysts.[11–13] Furthermore, Au NPs have been frequently discussed in terms of their applications in nano electronic devices,[14,15] or as switches[16] and sensors.[17] With regard to the latter, even theoretical studies were performed, supporting the experimental data[18] and revealing the use of functionalised Au NPs as colorimetric probes.[19,20] However, the by far most extensive usage of Au NPs is in the biomedical research. Here, Au NPs have recently been used as contrast agents for computer tomography (CT),[21,22] carrier for drug delivery[23,24] or photoacoustic imaging.[25] Furthermore, they have been studied as agents for photodynamic therapy (PDT)[26,27] or even used in immunoassays, when the Au NPs were functionalised with antibodies.[28–31] The synthesis of Au NPs is already well understood,[32] and they allow for an excellent size control. Moreover, their biocompatibility and their stability against oxidation and degradation *in vivo* represent additional advantages.[33]

NPs in general need to be sufficiently stabilised in order to prevent them from agglomeration. This occurs electrostatically with charged ligands or sterically with bulky ligands on the surface. By choosing the suitable ligand, it is possible to attach other desired compounds (such as bioactive molecules) onto the surface. Due to their enormous surface-to-volume ratio the NPs can be loaded with a large amount of these desired compounds.[34]

Au NPs which are functionalised with a variety of different biogenic substances as ligands show so-called multivalent receptor activations in biological systems.[35,36] In contrast to

[a]*Institute of Inorganic Chemistry, University of Cologne, Greinstrasse 6, 50939 Cologne, Germany*

[b]*Institute of Veterinary Physiology and Biochemistry, Justus Liebig University Giessen, Frankfurter Strasse 100, 35392 Giessen, Germany. E-mail: rebecca.classen@vetmed.uni-giessen.de*

[c]*Institute of Physiology, Justus Liebig University Giessen, Aulweg 129, 35392 Giessen, Germany*

† Electronic supplementary information (ESI) available: Synthetic procedures and characterisation of Au NPs. See https://doi.org/10.1039/d2na00171c

monovalent interactions, whereby only one receptor–ligand complex is formed at a certain time, in multivalent systems multiple molecular recognition events between biomolecules and receptors operate simultaneously. This leads not only to multiple and more intense interactions, even more influenced ligand–receptor recognition,[37] but also to a significant amplification of the effects at the receptor site.[38]

This key principle of multivalency was also investigated in the present study. In this work, we have functionalised Au NPs with the two catecholamines adrenaline and noradrenaline, which are also closely linked in their biosynthesis and in their chemical structure. Noradrenaline and adrenaline act as endogenous transmitter in the sympathetic nervous system,[39] yet while noradrenaline is a primary amine, adrenaline carries an additional methyl group on the nitrogen and thus represents a secondary amine. Both act as hormones with a catechol unit in their structure and thus cause a stimulation of adrenergic receptors.[40]

In our previously published work,[35,36] we observed multivalent effects in certain receptor activations caused by Au NPs functionalised with different biogenic amines such as histamine or carbachol. In case of carbachol functionalised Au NPs, a potentiation of the effects to a factor of over 10^6-fold could be determined. This observation was further supported by FRET measurements showing the actual activation of the G-proteins by carbachol functionalised Au NPs at picomolar concentrations.[34]

As adrenergic receptors mediate physiological responses in multiple organ systems such as *e.g.* epithelial secretion, smooth muscle contractions or cardiac functions, in the present study we tried to find out, whether it is possible to synthesise gold nanoparticles functionalised with adrenaline or noradrenaline and whether these NPs are able to interact with adrenergic receptors in different biological systems.

Results and discussion

Chemical syntheses

Catecholamines are different to the biogenic amines used in our previous work, as they tend to undergo an oxidation when being exposed to oxygen.[41] When dissolved in an aqueous medium oxidation occurs at the air–water-interface.[42] For this reason the preparation of functionalised Au NPs was performed *via* a different strategy during this work as pictured in Fig. 1.

First, the whole ligand was prepared separately using a bifunctional thiol ligand as a linking unit and the biogenic catecholamine. Afterwards the functionalisation on the pre-synthesised Au NPs took place. All synthetic steps including the catecholamines were performed under anaerobic conditions.

One part of this ligand represents a mercaptoacid, and this bifunctional compound is acting as a linking unit. On one side, an attachment onto the Au NP surface can be achieved *via* the thiol group due to the strong Au–S bond formed (HSAB principle). Furthermore, the acid function on the other end of the linker can be coupled to the desired biogenic amine by the formation of an amide bond. In this way, the biomolecules are derivatised in such a manner that linkage to the NPs is enabled. With the presence of a relatively strong amide bond formed, the attached biomolecule of interest should remain bonded to the NP until it reaches the point of action. Moreover, with the use of a long chain linker such as mercaptoundecanoic acid a steric stabilisation of the NPs is achieved.

Ligand syntheses

The syntheses were performed according to a modified version reported by Abed *et al.*[43] and are displayed in Scheme 1. Mercaptoundecanoic acid (MUDA) was stirred with *N*-hydroxylsuccinimide (NHS) and diisopropylcarbodiimide (DIC) dissolved in absolute pyridine under argon atmosphere at room temperature until the active ester with NHS was formed. The reaction is a well-established amide coupling, the mechanism of which has already been described frequently.[44,45] After 4 h the biogenic amine (either adrenaline (ADR) or noradrenaline (NA)) dissolved in pyridine was added. Mildly basic reaction conditions were achieved by the simultaneous addition of K_2CO_3 in degassed H_2O. The active ester reacts *in situ* with the amine to yield the amide.

Aqueous work ups were performed after thin layer chromatography (TLC) monitoring showed the complete consumption of the starting materials. Even after purification *via* column chromatography, traces of the side product *N*,*N*′-diisopropylurea (DIU) remained next to the pure product and could not be removed completely during various work up steps. Elemental analysis proved an equivalent of DIU present in the sample. Complete removal of DIU could only be achieved using preparative HPLC. However, as this side product is not of interest during the functionalisation step of the Au NPs, the presence of DIU was taken into account in the reaction as free

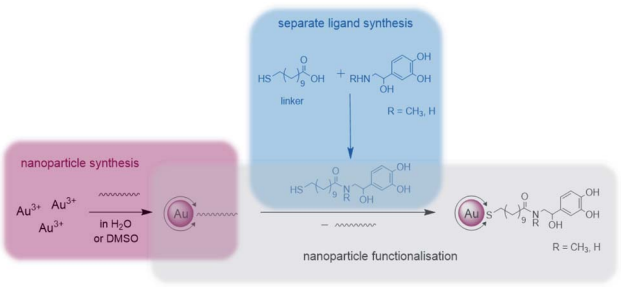

Fig. 1 Synthetic strategy during this work divided into the following sections: separate ligand synthesis (blue), nanoparticle synthesis (pink) and nanoparticle functionalisation (grey).

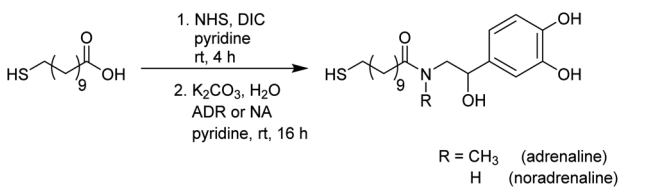

Scheme 1 Ligand syntheses with the biogenic amines adrenaline (ADR) and noradrenaline (NA).

molecules and side products can be removed afterwards *via* dialysis.

The desired biofunctional ligand possesses a thiol moiety which is more favourable to be attached to the NPs during a ligand exchange reaction than any DIU side product.

Both ligands, *i.e.* MUDA-ADR and MUDA-NA were further analysed *via* NMR, IR and ESI-MS. Attempts of crystallisation were also performed but without any success. ^{1}H-NMR spectra show all predicted proton resonances of the desired ligand. The aromatic protons of the biogenic amines (ADR or NA) have resonances between 6.76 ppm and 6.52 ppm. Furthermore, the ligands show intense resonances in the range from 1.57 ppm to 1.17 ppm which can be assigned to the long alkyl chain of the thiol linker (MUDA).

IR spectroscopy was performed to additionally verify the existing binding types within the ligands. The IR spectra of MUDA-ADR and MUDA-NA both show a strong ν_{O-H} band at *ca.* 3300 cm^{-1} indicating the presence of hydroxy groups. Carbonyl bands of the amides are in the range between 1650 cm^{-1} and 1600 cm^{-1}. These bands, together with δ_{C-N} vibrations around 1240 cm^{-1}, confirm the formation of amide bonds. Furthermore, a small ν_{N-H} band can be observed for MUDA-NA around 3100 cm^{-1}. This band does not exist in the MUDA-ADR spectrum, as MUDA-ADR lacks an NH-group due to its *N*-methylation.

The molecular masses were confirmed using ESI MS. The molecule ion $[M - H]^-$ of 380.20 was found for MUDA-ADR and $[M - H]^-$ of 368.20 for MUDA-NA. Both match with the calculated ligand masses.

Gold nanoparticle syntheses

Since these NPs were prepared in order to use them for biomedical applications, their homogeneity and comparability amongst each other was a significant point to be addressed. Thus, to obtain monodispersive Au NPs during the synthesis was a crucial step. In this work two different wet chemical *bottom up* methods were used which provided very good results in size control as well as easily applicable techniques. As described in our previous publications, the Au NPs synthesis using the citrate reduction method by Frens[46] is readily reproducible in aqueous media and yields Au NPs with an average size of 14 nm.[17] In accordance, we have reacted the gold precursor with citrate only (operating as both a reducing agent and a stabilising agent simultaneously) and obtained Au NPs as pictured in Scheme 2A. Since citrate only offers a weak reducing character, the obtained NPs possess relatively large diameters (>10 nm). Au-citrate NPs sized smaller than 10 nm synthesised according to the Turkevich method are very rarely known in the literature.[47] Moreover, Au-citrate NPs allow only rather low concentrations (around 10 nM), since citrate molecules offer only a light stabilising character and thus agglomeration would occur at higher concentrations. In order to obtain smaller Au NPs with a higher concentration, we used a modified version of Stucky and coworkers[48] with t_{Bu}-amine borane complex as a stronger reducing agent. A very narrow size distribution and furthermore a very good size control could be achieved in the synthesis using mercaptoundecanoic acid (MUDA) as the capping agent in DMSO as a solvent (Scheme 2B).

The resulting Au NPs were more stable than those obtained using the citrate reduction method, and thus they were purified via centrifugation. After this step, the Au NPs were redispersed in H_2O and dialysed against H_2O for further purification. With changing the ratios of added starting materials, different core sizes of the NPs could be obtained. A following tendency could be observed with regard to the size control: the larger the equivalent of reducing agent added, the smaller the sizes of the formed Au NPs.

All of the obtained Au NP solutions were characterised with different methods. Using transmission electron microscopy (TEM) and ultraviolet-visible spectroscopy (UV-Vis) the metallic nanoparticle core can be investigated. Dynamic light scattering (DLS) gives information about the whole nanoparticle when measuring the hydrodynamic diameter. With nuclear magnetic resonance spectroscopy (NMR) and infrared spectroscopy (IR) the structure of the organic framework can be analysed.

TEM images of the obtained NPs show predominantly spherical NPs with a narrow size distribution and without visible agglomeration. Au-citrate NPs (shown in Fig. 2A) possessed an average diameter of $d_{TEM} = 13.8 \pm 1.2$ nm. In contrast, the largest Au NPs prepared *via* the modified Stucky method had an average diameter of $d_{TEM} = 9.7 \pm 1.0$ nm when the ratio of PPh_3AuCl : MUDA : t_{Bu}-amine borane was set to 1.0 eq. : 0.7 eq. : 0.7 eq. (Au-MUDA Ø 10 nm, Fig. 2B). Even smaller NPs with a more narrow size distribution could be obtained using the same method with a PPh_3AuCl : MUDA : t_{Bu}-amine borane ratio of 1.0 eq. : 4.6 eq. : 10 eq. with an average diameter of $d_{TEM} = 7.9 \pm 0.7$ nm (Au-MUDA Ø 8 nm, Fig. 2C).

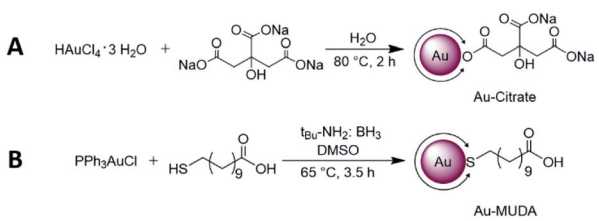

Scheme 2 Au NP synthesis *via* (A) the citrate reduction method according to Mattern *et al.*[17] yielding in 14 nm Au-citrate NPs and (B) a modified version of Stucky *et al.*[30] in order to obtain slightly smaller Au-MUDA NPs between 8–10 nm.

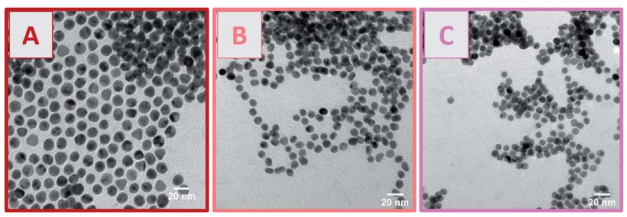

Fig. 2 TEM images of (A) Au-citrate $d = 13.8 \pm 1.2$ nm, (B) Au-MUDA $d = 9.7 \pm 0.9$ nm and (C) Au-MUDA $d = 7.9 \pm 0.9$ nm show monodispersive Au NPs.

Table 1 Properties of the synthesised Au NPs including the ratios of starting materials used

Size	8 nm (Au-MUDA)	9 nm (Au-MUDA)	10 nm (Au-MUDA)	14 (Au–citrate)
Au precursor	1.0 eq.	1.0 eq.	1.0 eq.	1.0 eq.
Ligand	4.6 eq.	1.0 eq.	0.7 eq.	5.8 eq.
Reducing agent	10 eq.	10 eq.	0.7 eq.	
TEM	$d = 7.9 \pm 0.9$ nm	$d = 9.0 \pm 0.9$ nm	$d = 9.7 \pm 1.0$ nm	$d = 13.8 \pm 1.2$ nm
DLS	$d_{hydr} = 12 \pm 3$ nm	$d_{hydr} = 14 \pm 4$ nm	$d_{hydr} = 12 \pm 3$ nm	$d_{hydr} = 15 \pm 3$ nm
UV/Vis	$\lambda_{max} = 528$ nm	$\lambda_{max} = 526$ nm	$\lambda_{max} = 525$ nm	$\lambda_{max} = 521$ nm
Concentration c	212 nM	143 nM	115 nM	7.8 nM

Table 1 lists different characteristics of the synthesised Au NPs. In addition to their diameter d_{TEM} we also determined the hydrodynamic diameter d_{hydr} using DLS showing always slightly larger d_{hydr} than their corresponding d_{TEM} sizes. This is due to the fact that DLS considers the entire NP with ligand shell, whereas in TEM only the gold core of the NP can be measured.

All listed concentrations were determined with the yielded sizes as well as the quantity of gold precursors used. Important to mention is that this consideration is based on the assumption that the precursors are completely reduced to NPs.

Since Au NPs have a distinctive plasmon resonance, they can be further characterised by UV/Vis spectroscopy. The measured absorptions of all synthesised pink and clear Au NP samples are displayed in Fig. 3. Au-citrate has its absorption maximum (λ_{max}) at 521 nm. Various ligands on the surface of a NP can influence the position of λ_{max}. A bathochromic shift of λ_{max} towards larger wavelengths can be observed for Au NPs synthesised and stabilised with the long chain ligand MUDA. For Au-MUDA (Ø 10 nm) a λ_{max} of 525 nm was measured. The UV/Vis spectrum of Au-MUDA (Ø 8 nm) shows an absorption maximum λ_{max} at 527 nm. These measurements show a trend in the position of the absorption maximum indicating a bathochromic shift for smaller sized nanoparticles.

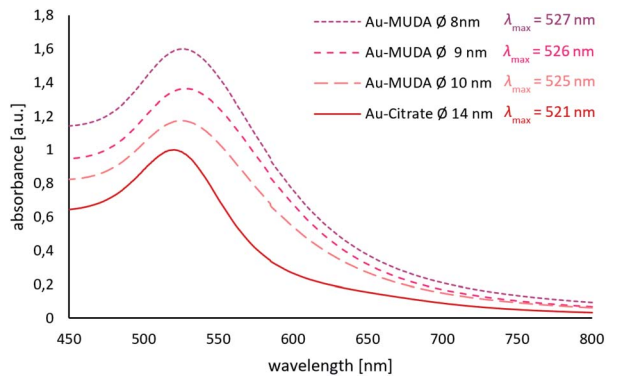

Fig. 3 UV/Vis spectra of Au-MUDA Ø 8 nm, Ø 9 nm, Ø 10 nm and Au-citrate Ø 14 nm with their measured absorption maxima.

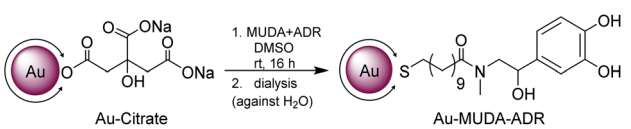

Scheme 3 Nanoparticle functionalisation in a ligand exchange reaction with the presynthesised catecholamine carrying ligands (MUDA-ADR or MUDA-NA), shown here with MUDA-ADR as an example.

Nanoparticle functionalisation

In the final step the functionalisation of the presynthesised Au NPs took place using ligand exchange reactions with the synthesised catecholamine carrying ligands (MUDA-ADR or MUDA-NA), shown in Scheme 3.

The Au NP solution of the preferred size was degassed with argon prior to the addition of the ligand. The ligand itself was dissolved in DMSO and added dropwise under vigorous stirring in order to obtain a rapid intermixing. Thereby it is beneficial to add the ligand dissolved in the respective solvent in order to avoid agglomeration of the Au NPs upon the addition of bulk material. The ligand was added in a large excess (up to 8×10^6-fold) in order to induce a high ligand exchange.

To ensure a stable Au NP solution during the reaction, the pH was adjusted to 8 by adding NEt_3. The resulting pink clear

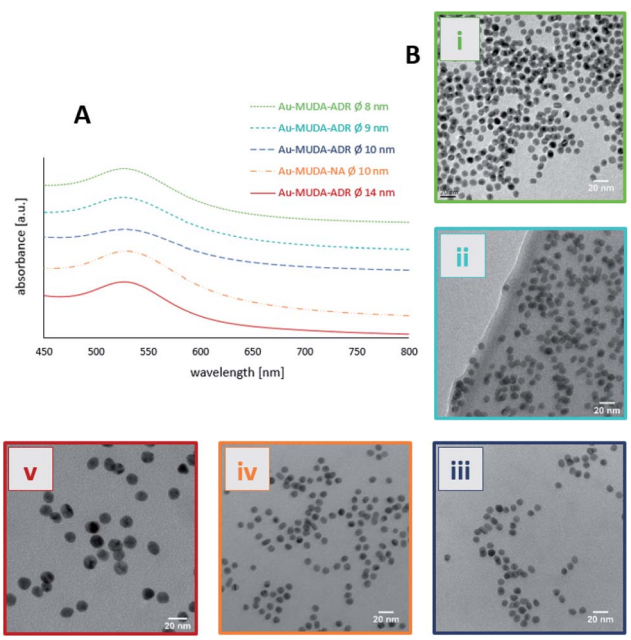

Fig. 4 (A) UV/Vis spectra of the functionalised Au NPs Au-MUDA-ADR Ø 14 nm, Ø 10 nm, Ø 9 nm, Ø 8 nm and Au-MUDA-NA Ø 10 nm with their measured absorption maxima, and (B) their corresponding TEM images of (i) Au-MUDA-ADR $d = 8.1 \pm 0.6$ nm, (ii) Au-MUDA-ADR $d = 8.9 \pm 0.8$ nm, (iii) Au-MUDA-ADR $d = 9.9 \pm 0.9$ nm, (iv) Au-MUDA-NA $d = 9.9 \pm 0.8$ nm and (v) Au-MUDA-ADR $d = 13.9 \pm 1.2$ nm.

Table 2 Properties of the synthesised functionalised Au NPs

Size	8 nm	9 nm	10 nm	14 nm	10 nm
Sample	Au-MUDA-ADR				Au-MUDA-NA
d_{TEM}/nm	8.1 ± 0.6	8.9 ± 0.8	9.9 ± 0.9	13.9 ± 1.2	9.9 ± 0.8
d_{hydr}/nm	17 ± 5	13 ± 3	13 ± 5	16 ± 4	17 ± 4
λ_{max}/nm	526	525	523	525	528
Concentration c	157 nM	191 nM	101 nM	7.1 nM	35 nM

and stable Au NPs solution was then directly purified *via* dialysis. Dialysis was chosen as a gentle and biocompatible purification method. In this way, remaining free ligands which are not coated on the NP and other side products could be removed from the solution.

TEM images proved that no change in the morphology of the NPs occurred during their functionalisations (Fig. 4B(i)–(v)). Spherical Au NPs remain present in their desired diameters with a remarkable small size distribution. Moreover, no agglomeration of the functionalised Au NPs could be observed. Next to the TEM investigations also DLS measurements were performed (displayed in Table 2) showing that the determined d_{hydr} remain in the appropriate range and thus support the conclusion that a stable NP solution is present.

All of the pink and clear Au NP samples were further characterised *via* UV/Vis showing a slight bathochromic shift in the measured absorption maxima (Fig. 4A). Yet, the existence of just one plasmon resonance with λ_{max} in the region around 520 nm confirm the successful synthesis of spherical stable Au NP solutions in these size regions.

The organic surface structures of the Au NPs were further analysed using IR and NMR spectroscopy in order to confirm that the ligand exchanges during each functionalisation reaction have been successful.

IR spectra were recorded with dried samples of the Au NPs. The measured spectra of functionalised Au NPs were compared to spectra of the starting Au NP solutions (Au-citrate and Au-MUDA) as well as the synthesised ligands (MUDA-ADR or MUDA-NA). Even though the Au NP samples were dried, a broad OH band around 3000 cm^{-1} can be observed in the spectra, indicating that the Au NPs still possess residual H_2O trapped. However, more importantly, the bands assigned to the desired ligand are also present in the spectra of functionalised Au NPs (Au-MUDA-ADR and Au-MUDA-NA). A broad ν_{O-H} band at *ca.* 3300 cm^{-1} is assigned to the hydroxyl groups. Furthermore, the desired amide bonds can be observed around 1600 cm^{-1} for $\nu_{C=O}$ and δ_{N-H} as well as δ_{C-N} vibrations around 1250 cm^{-1}.

Moreover, ^{1}H-NMR spectra of all functionalised samples were recorded. The Au NP solution was dried *in vacuo* and subsequently dissolved in D_2O in order to prepare the samples. To ensure stable solutions during the measurements, a base (NEt_3 or NaOH) in D_2O was added. The measured NMR spectra were then compared to the spectra of the initial Au NP solutions as well as the synthesised ligands.

Although the quality of a measured Au NP ^{1}H-NMR spectrum is affected by the extremely small sample quantity as well as the appearance of line broadening and shifting due to the inherent physical nature of the NPs,[49] it was possible to assign the proton signals of the synthesised ligands (MUDA-ADR or MUDA-NA) on the Au NP surface. In sum, these data unambiguously prove the successful functionalisation of Au NPs with the catecholamines adrenaline and noradrenaline.

Biological actions of nanoparticles functionalised with adrenaline

In a first attempt to study the biological activity of Au NPs functionalised with adrenaline, the effect of Au-MUDA-ADR (Ø 9 nm) on ion transport across rat distal colonic epithelium was studied. In this tissue, native adrenaline (ADR) evokes a K^+ secretion leading to a negative short-circuit current (I_{sc}) *via* stimulation of both β_1- and β_2-receptors.[50,51] Indeed, Au-MUDA-ADR (5 nmol l^{-1} at the serosal side) induced a current of −0.26 ± 0.06 μEq h^{-1} cm^{-2} ($p < 0.05$ *versus* baseline just prior administration of Au-MUDA-ADR, $n = 7$; Fig. 5A), which was completely prevented, when the tissue was pretreated with the nonselective β-receptor blocker bupranolol (10 μmol l^{-1} at the serosal side; $n = 8$; Fig. 5B). At the end of the experiment, the cholinergic agonist carbachol (50 μmol l^{-1} at the serosal side) was administered as viability control. The cholinergic agonist evokes a strong Cl^- secretion, thereby leading to an increase in I_{sc}. This increase in I_{sc} amounted to 10.76 ± 1.94 μEq h^{-1} cm^{-2}

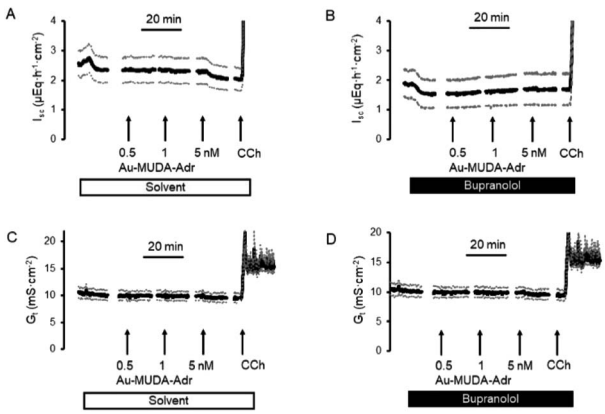

Fig. 5 (A, B) Au-MUDA-ADR NP (0.5–5 nmol l^{-1} at the serosal side administered in a cumulative manner) induced a negative I_{sc} in rat colonic epithelium (A), which was suppressed by preincubation with the nonselective β-blocker bupranolol (10 μmol l^{-1} at the serosal side (B)). The control tissues (A) were treated with the same volume of the solvent (ethanol) as used in B for the administration of bupranolol. At the end of each experimental series, carbachol (CCh; 50 μmol l^{-1} at the serosal side) was administered as viability control. (C, D) Tissue conductance (G_t) was not altered by Au-MUDA-ADR. Data are means (thick line) ± SEM (dotted lines), $n = 7$–8.

($n = 7$) in the control series (Fig. 5A) and to 9.12 ± 1.30 μEq h^{-1} cm^{-2} ($n = 8$) after pretreatment with bupranolol (Fig. 5B) thus excluding that the inhibition of the Au-MUDA-ADR NP response by bupranolol might be caused by a nonspecific inhibition of epithelial transport processes. Also tissue conductance, a measure for the ionic permeability of the epithelium and a sensitive indicator for epithelial damage was unaltered by Au-MUDA-ADR (Fig. 5C and D), whereas carbachol induced a prompt increase in G_t due to opening of Cl^- channels in the apical membrane of the epithelial cells.

An interesting medical issue for application of NPs functionalised with adrenaline (ADR) might be the respiratory tract, where stimulation of β_2-receptors on smooth muscle cells is one of the main drug targets used in the therapy of asthma, as stimulation of these receptors induces a bronchodilation.[52] Therefore, contractility of the upper respiratory tract was measured under isometric conditions after precontraction induced by the cholinergic agonist carbachol (0.5 μmol l^{-1}). Native adrenaline (10–1000 μmol l^{-1}) induced a prompt, concentration-dependent relaxation (Fig. 6A; $n = 8$). This relaxation was inhibited, when adrenaline was administered in the presence of the β_2-receptor blocker ICI-118551 (10 μmol l^{-1}; Fig. 6B; $n = 5$). At the lowest concentration tested, the relaxation induced by the adrenergic agonist was even reverted into a contraction suggesting a stimulation of α-receptors[53] under these conditions. In contrast, Au-MUDA-ADR in a concentration of up to 10 nmol l^{-1} (*i.e.* 2× the concentration effective in the Ussing chamber experiments; Fig. 5A) induced – after a transient contractile response – a slow fall in muscle tone (Fig. 6C; $n = 5$), which was not altered after preincubation with ICI-118551 (10 μmol 1^{-1}; Fig. 6D; $n = 5$). At the end of each experimental series, a viability control (not shown) was performed with KCl (30 mmol l^{-1}), which caused an increase in muscle force by 0.33 ± 0.08 g ($n = 5$) in the series of experiments without ICI-118551

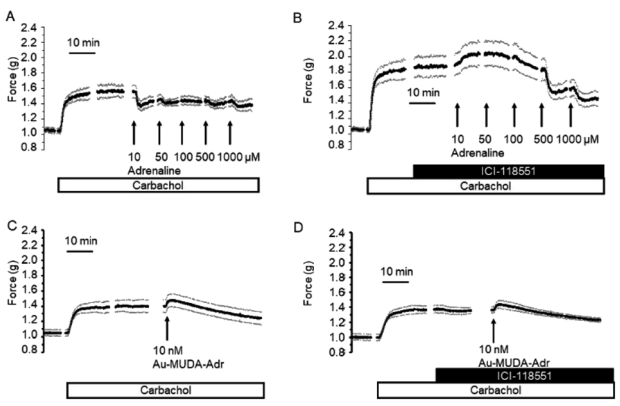

Fig. 6 Concentration-dependent relaxation of segments from rat upper respiratory tract by adrenaline; (10–1000 μmol l^{-1}; arrows) under control conditions (A) and after pretreatment (B) with the β_2-blocker ICI-118551 (10 μmol l^{-1}; black bar). Missing effect of Au-MUDA-ADR (10 nmol l^{-1}; arrows) under control conditions (C) or after pretreatment (D) with ICI-118551 (10 μmol l^{-1}; black bar). All segments were precontracted with the cholinergic agonist carbachol (0.5 μmol l^{-1}; white bar). Data are means (thick line) ± SEM (dotted lines), $n = 5$–8.

Table 3 Properties (size, conjugated adrenergic agonist) of the functionalised nanoparticles tested for their ability to relax segments from rat upper respiratory tract precontracted by carbachol (0.5 μmol l^{-1}) under isometric conditions

Nanoparticle conjugated with	Size	Effect at smooth muscle from the respiratory tract
Adrenaline	8 nm	None
Adrenaline	9 nm	None
Adrenaline	10 nm	None
Adrenaline	14 nm	None
Noradrenaline	10 nm	None

and 0.34 ± 0.04 g ($n = 5$) in the series with ICI-118551 demonstrating the viability of the preparations.

In order to find out, whether the missing effect on β_2-receptors of adrenaline functionalised Au NPs might be caused by unfavourable spatial conditions, different sizes of the gold core ranging from 8 to 14 nm were tested (Table 3). However, none of the tested nanoparticles induced a significant relaxation at the isolated rings from the respiratory tract. This was also the case with noradrenaline functionalised Au NP (Au-MUDA-NA (Ø 10 nm)).

The missing effect of Au-MUDA-ADR at smooth muscle from the respiratory tract suggests that the induction of K^+ secretion by the functionalised nanoparticles might be caused by a stimulation of β_1-receptors. In order to test this hypothesis, contractility studies were performed at isolated rat cardiomyocytes, where β_1-receptors exert a positive inotropic effect and thereby increase cellular contraction during electrical stimulation. Isoprenaline (10 nmol l^{-1}), a nonselective β-agonist, caused a strong increase in cellular shortening (dL/L) by 43.1 ± 1.8% ($n = 216$), a response which was suppressed by prior incubation of the cardiomyocytes with the β_1-receptor blocker atenolol (10 μmol l^{-1}). Atenolol alone did not change contractility (Fig. 7B). Au-MUDA-ADR (Ø 9 nm) indeed increased

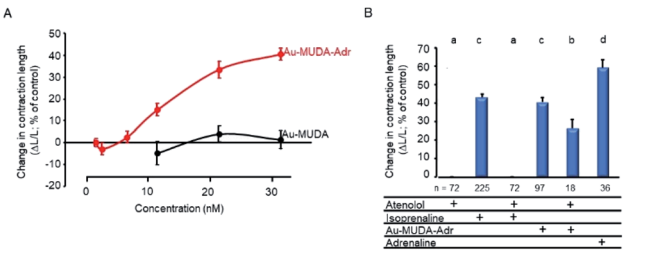

Fig. 7 (A) Concentration-dependent increase in contractility of isolated rat cardiomyocytes (measured as cell shortening) by Au-MUDA-ADR (red symbols; $n = 53$–81), but not by Au-MUDA without adrenaline (black symbols; $n = 27$–36). (B) Effects of different adrenergic agonists and antagonists on contractility. Concentrations used were: atenolol (10 μmol l^{-1}), isoprenaline (10 nmol l^{-1}), Au-MUDA-ADR (30 nmol l^{-1}), and adrenaline (5 μmol l^{-1}). In each cell culture dish, only one drug or drug combination was tested. All data are expressed as relative changes in cell length evoked by electrical stimulation under control conditions, where electrical stimulation evoked a reduction in cell length by 9.16 ± 0.17% ($n = 216$), which was set as reference value (100%) for all data. Data are means (symbols or bars, respectively) ± SEM (lines). Letters (a–d) indicate statistically homogenous groups.

cellular shortening in a concentration-dependent manner, *i.e.* exerted a positive inotropic action, which was not observed for Au-MUDA not functionalised with the catecholamine (Fig. 7A). The increase in contractility induced by the highest concentration used of Au-MUDA-ADR (30 nmol l^{-1}) reached about 2/3 of the increase in contractility induced by native adrenaline (5 μmol l^{-1}). The stimulatory effect of Au-MUDA-ADR was significantly inhibited by pretreatment with atenolol. Inhibition was less in comparison to the inhibition of the isoprenaline response induced by atenolol, which might be explained by the assumed higher affinity of multivalently administered adrenaline present in high local density on the gold cores of the NPs. It must be noted that in the combined presence of atenolol and Au-MUDA-ADR, in several culture dishes electrically evoked contractions ceased in the prolonged presence of both drugs which might indicate a reduced cell viability under these conditions of prolonged β-receptor stimulation.

Conclusions

In conclusion, the present experiments demonstrate that it is possible to immobilise different adrenergic agonists onto gold nanoparticle surfaces *via* mercaptoundecanoic acid as a linking unit. These nanoparticles show biological activity in the nanomolar range in various biological systems, where β_1-adrenergic receptors are involved in the control of physiological processes such as intestinal secretion or cardiac contractility. They are ineffective at β_2-adrenergic receptors involved in the control of smooth muscle contractility suggesting that the Au-MUDA moiety might spherically impair the activation of these types of receptors by the adrenergic agonists present on the surface of the nanoparticles. β_1-and β_2-adrenergic receptors use the same binding pocket for catecholamines. However, there are differences in the form and electrostatic properties of the extracellular vestibule of these two receptors which limit the access to the binding pocket.[54] These spherical differences might be responsible for the present observations that adrenaline bound on the surface of gold nanoparticles might reach the binding pocket of β_1-, but not of β_2-adrenergic receptors. Agonists of G-protein coupled receptors bound on nanoparticles show a strong increase in affinity compared to single molecule agonists, a phenomenon, which is due to multivalent interaction with receptors. Therefore, it will be important in the future to study changes in binding behaviour such as determinations of on constants (k_{on}) and off constants (k_{off}) *e.g.* in ligand binding assays using radiolabelled functionalised nanoparticles[55] or isothermal titration calorimetry to get deeper insights in the mechanisms of action of multivalency.

Experimental

All chemicals were purchased from Acros Organics, Alfa Aesar, Carl Roth, Fluka, Santa Cruz Biotechnology, Sigma Aldrich or TCI and used without further purification. Adrenaline was purchased as (−)-epinephrine (+)-bitartrate (98+%) from Acros Organics and noradrenaline as (±)-norephinephrine (+)-bitartate from Sigma Aldrich. Organic solvents were distilled before use or purchased in an anhydrous state and stored over molecular sieves. Chromatographic purifications were performed using Merck silica gel 60 (0.040–0.063 mm). Thin layer chromatography (TLC) was performed on Merck aluminium-backed plates with silica gel and fluorescent indicator (254 nm). For indicating, UV light (λ = 254 nm/365 nm) was used. Reactions were performed under inert conditions (argon atmosphere 99.9999%, Air Products) using standard Schlenk line techniques with oven dried glassware, unless stated differently.

All water-based (nanoparticle) syntheses were performed in demineralised water. All glass vessels were washed with aqua regia and demineralised water prior to use. For dialysis of the NP solutions, membranes of regenerated cellulose "ZelluTrans" with different pore sizes (MWCO 12 000) by Carl Roth GmbH were used. The dialysis membrane was immersed in the dialysing solvent for 30 min prior to use. All dialyses were performed at room temperature (in air).

^{1}H NMR and ^{13}C NMR spectra were recorded on Bruker Avance 400 MHz (AV 400) und Bruker Avance II+ 600 MHz (AV II 600) spectrometers at the NMR platform of the chemistry department of the University of Cologne. All measurements were performed at room temperature. Chemical shifts are given in ppm relative to respective solvent peaks. ^{1}H NMR data are reported as follows: chemical shifts (multiplicity [ppm], classification). Multiplicity is recorded as s = singlet, d = doublet, t = triplet, q = quartet, m = multiplet. IR measurements were performed on a PerkinElmer FTIR-ATR (UATR TWO) in the ATR mode. TEM images were taken on a Zeiss LEO 912 (300 kV, LaB6-cathode) equipped with a GATAN digital camera. For sample preparation, a 10 μl NP solution was placed on a carbon-coated copper grid. Determination of the average particle size and standard deviation was achieved by measuring 100 individual particles. Dynamic light scattering (DLS) measurements were performed on a NanoZS from Malvern. UV/Vis spectra were recorded with an UV-1600PC spectrophotometer from VWR.

Chemical syntheses

Synthesis of MUDA-ADR. Ligands were synthesised according to a modified version by Abed *et al.*[43] Mercaptoundecanoic acid (MUDA) (131 mg, 0.6 mmol, 1.0 eq.) and *N*-hydroxylsuccinimide (NHS) (55 mg, 0.48 mmol, 0.8 eq.) were dissolved in anhydrous pyridine (4 ml). The coupling reagent *N*,*N*′-diisopropylcarbodiimide (DIC) (112 μl, 0.72 mmol, 1.2 eq.) was added quickly and the solution was stirred at room temperature for 4 h under argon atmosphere. Potassium carbonate (K_2CO_3) (91 mg, 0.66 mmol, 1.1 eq.) in degassed water (H_2O) (0.5 ml) was added to a solution of epinephrine (+)-bitartrate (200 mg, 0.6 mmol, 1.0 eq.) in anhydrous pyridine (0.5 ml) which was then quickly added to the reaction solution and stirred at room temperature for 16 h under argon atmosphere. During the work up the reaction mixture was filtered, demineralised H_2O (5 ml, pH = 5 [with $NaHSO_4$]) was added and the solution was extracted with EtOAc (3 × 10 ml). The combined organic layers were washed with demineralised H_2O (15 ml), dried over Na_2SO_4 and filtered. The solvent was evaporated and the residue

was purified *via* column chromatography (EtOAc/$CHCl_3$ 4 : 1). The product could be obtained as a colourless solid in a moderate yield (175 mg, 76%) and stored at 4 °C in the dark.

^{1}H-NMR (499 MHz, DMSO-d_6): δ/ppm = 8.83–8.78 (m, 1H, O*H*), 8.77–8.67 (m, 1H, O*H*), 6.76–6.72 (m, 1H, C*H*), 6.69–6.64 (m, 1H, C*H*), 6.59–6.52 (m, 1H, C*H*), 5.34–5.11 (m, 1H, O*H*), 4.58–4.51 (m, 1H, C*H*), 3.24–3.16 (m, 1H, S*H*), 2.88–2.78 (m, 3H, CH_3), 2.48–2.42 (m, 2H, CH_2), 2.23–2.16 (m, 2H, CH_2), 1.57–1.44 (m, 4H, CH_2), 1.36–1.29 (m, 2H, CH_2), 1.28–1.19 (m, 12H, CH_2); ^{13}C{^{1}H} NMR (100 MHz, $CDCl_3$): δ/ppm = 172.6, 146.1, 145.3, 135.2, 119.1, 115.4, 71.3, 47.2, 43.6, 36.5, 34.5, 32.9, 32.2, 30.7, 30.5, 29.3, 28.5, 25.2, 24.9; IR (ATR): ν/cm^{-1} = 3333 (ν_{O-H}), 2921 (ν_{C-H}), 2846, 1735 ($\nu_{C=O}$), 1608 (δ_{N-H}), 1526 (ν_{C-H} + δ_{C-N-H}), 1451 ($\nu_{C=C}$), 1393 (δ_{C-H}), 1368 (δ_{O-H}), 1278 (δ_{C-N}), 1195 (ν_{C-O}), 1105, 1008, 872, 820, 752 (δ_{C-H}), 625 (ν_{C-S}); ESI-MS (*m*/*z*): $[M - H]^-$ = 382.13 (calcd: $[M - H]^-$ = 382.21); elemental analysis: anal. calcd for $(C_{20}H_{33}NO_4S)_1(C_7H_{16}N_2O)_{1.5}$: C, 61.07; H, 9.58; N, 9.34; S, 5.34. Found: C, 60.31; H, 9.91; N, 10.27; S, 5.53.

Synthesis of MUDA-NA. MUDA (52 mg, 0.24 mmol, 1.0 eq.) and NHS (22 mg, 0.19 mmol, 0.8 eq.) were dissolved in anhydrous pyridine (4 ml). The coupling reagent DIC (43 µl, 0.28 mmol, 1.2 eq.) was added quickly and the solution was stirred at room temperature for 4 h under argon atmosphere. K_2CO_3 (35 mg, 0.26 mmol, 1.1 eq.) in degassed H_2O (0.5 ml) was added to a solution of (±)-norephinephrine (+)-bitartate (75 mg, 0.24 mmol, 1.0 eq.) in anhydrous pyridine (0.5 ml) which was then quickly added to the reaction solution and stirred at room temperature for 16 h under argon atmosphere. During the work up the reaction mixture was filtered, demineralised H_2O (5 ml, pH = 5 [with $NaHSO_4$]) was added and the solution was extracted with EtOAc (3 × 10 ml). The combined organic layers were washed with demineralised H_2O (15 ml), dried over Na_2SO_4 and filtered. The solvent was evaporated and the residue was purified *via* column chromatography (EtOAc/$CHCl_3$ 4 : 1). The product could be obtained as a colourless solid in a moderate yield (57 mg, 67%) and stored at 4 °C in the dark.

^{1}H NMR (499 MHz, DMSO-d_6): δ/ppm = 8.88–8.61 (m, 2H, O*H*), 7.73 (t, 1H, N*H*, $^3J_{H-H}$ = 6.3 Hz), 6.72 (s, 1H, C*H*), 6.65 (d, 1H, C*H*, $^3J_{H-H}$ = 8.2 Hz), 6.54 (d, 1H, C*H*, $^3J_{H-H}$ = 8.2 Hz), 5.20 (s, 1H, O*H*), 4.41–4.36 (m, 1H, C*H*), 3.23–3.16 (m, 1H, S*H*), 2.48–2.43 (m, 2H, CH_2), 2.04 (t, 2H, CH_2, J_{H-H} = 7.4 Hz), 1.56–1.49 (m, 2H, CH_2), 1.48–1.41 (m, 2H, CH_2), 1.36–1.29 (m, 2H, CH_2), 1.28–1.17 (m, 12H, CH_2); 13C{1H} NMR (100 MHz, $CDCl_3$): δ/ppm = 173.0, 145.3, 144.6, 135.2, 115.5, 113.8, 71.6, 47.4, 36.3, 34.1, 29.5, 29.4, 29.3, 29.3, 29.2, 29.1, 28.9, 25.7, 24.2; IR (ATR): ν/cm^{-1} = 3341 (ν_{O-H}), 3116 (ν_{N-H}), 2965, 2919 (ν_{C-H}), 2846, 1705 ($\nu_{C=O}$), 1615 (δ_{N-H}), 1555 (ν_{C-H} + δ_{C-N-H}), 1465 ($\nu_{C=C}$), 1382 (δ_{C-H}), 1360 (δ_{O-H}), 1240 (δ_{C-N}), 1165 (ν_{C-O}), 872, 805 (δ_{C-H}), 625 (ν_{C-S}); ESI-MS (*m*/*z*): $[M - H]^-$ = 368.20 (calcd: $[M - H]^-$ = 368.19); elemental analysis: anal. calcd for $(C_{19}H_{31}NO_4S)_1(C_7H_{16}N_2O)_{1.5}$: C, 60.48; H, 9.46; N, 9.56; S, 5.47. Found: C, 59.63; H, 10.20; N, 10.85; S, 5.07.

Synthesis of citrate coordinated Au NPs (Au-citrate Ø 14 nm). Au-citrate NPs were synthesised according to the Turkevich method modified and previously published by Mattern *et al.*[35] Tetrachloroauric acid trihydrate ($HAuCl_4 \cdot 3H_2O$) (50 mg, 0.13 mmol) was dissolved in demineralised H_2O (198 ml) and heated to reflux for 20 min. A solution of trisodium citrate dihydrate (224 mg, 0.76 mmol) in demineralised H_2O (2 ml) was added quickly under vigorous stirring. The solution was heated to 80 °C for 2 h before cooling in an ice bath and filtrated using syringe filtration on a cellulose membrane with 0.2 µm pore size. A dark red, clear NP solution with a particle concentration of 7.8 nM was obtained and stored at 4 °C in the dark.

^{1}H-NMR (600 MHz, D_2O): δ/ppm = 2.71–2.69 (m, 2H, CH_2), 2.61–2.58 (m, 2H, CH_2); IR (ATR): ν/cm^{-1} = 3425 (ν_{O-H}), 1595 ($\nu_{C=O}$), 1249, 620; TEM: d = 13.8 ± 1.2 nm; UV/Vis: λ_{max} = 521 nm; DLS: d_{hydr} = 15 ± 3 nm (PDI = 0.04).

General synthetic procedure for mercaptoundecanoic acid coordinated gold nanoparticles (Au-MUDA)

Au-MUDA NPs were obtained in a direct synthesis according to modified version of the Stucky method.[48] Chloro(triphenylphosphine)gold(I) (PPh_3AuCl) was dissolved in dimethyl sulfoxide (DMSO) (3 ml) and a solution of the mercaptoundecanoic acid (MUDA) dissolved in DMSO (1 ml) was added. The mixture was heated to 65 °C and a solution of t_{Bu}-amine borane complex in DMSO (1 ml) was added quickly under vigorous stirring. The dark red solution was stirred at 65 °C for 3.5 h in the dark before cooled in an ice bath. Subsequently, the particles were precipitated with ethanol (EtOH) (10–14 ml) and centrifuged (45 min, 7000 rpm). The supernatant was discarded, the dark residue was redispersed three times and washed again with EtOH. The obtained dark solid was dried in air and redispersed in water (10 ml). Diluted NaOH (0.1–0.2 ml) was added to obtain a stable nanoparticle solution. Then, the solution was further purified *via* dialysis against H_2O.

Synthesis of Au-MUDA (Ø 8 nm) in H_2O. PPh_3AuCl (16 mg, 31 µmol, 1.0 eq.) in DMSO (3 ml), MUDA (30 mg, 138 µmol, 4.6 eq.) in DMSO (1 ml), t_{Bu}-amine borane (27 mg, 300 µmol, 10 eq.) in DMSO (1 ml).

The dark solid was redispersed in H_2O (10 ml). Diluted NaOH (2 drops) were added to obtain a stable NP solution which was further purified *via* dialysis against demineralised H_2O (in MWCO 12 000, 24 h). The violet, clear NP solution with a particle concentration of 212 nM, was stored at 4 °C in the dark.

^{1}H-NMR (600 MHz, D_2O): δ/ppm = 2.93–2.86 (m, 2H, CH_2), 2.17 (t, J = 6.6 Hz, 2H, CH_2), 1.75–1.68 (m, 2H, CH_2), 1.58–1.50 (m, 2H, CH_2), 1.45–1.36 (m, 2H, CH_2), 1.36–1.24 (m, 10H, CH_2); IR (ATR): ν/cm^{-1} = *ca.* 3300 (ν_{O-H}, H_2O), 2921 (ν_{C-H}), 2846 (ν_{C-H}), 1675, 1555 ($\nu_{C=O}$), 1533, 1443, 1406 (δ_{C-H}), 1293 (ν_{C-O}), 955, 723 (δ_{C-H}); TEM: d = 7.9 ± 0.9 nm; UV/Vis: λ_{max} = 527 nm; DLS: d_{hydr} = 12 ± 3 nm (PDI = 0.06).

Synthesis of Au-MUDA (Ø 9 nm) in H_2O. PPh_3AuCl (16 mg, 31 µmol, 1.0 eq.) in DMSO (3 ml), MUDA (7 mg, 30 µmol, 1.0 eq.) in DMSO (1 ml), t_{Bu}-amine borane (27 mg, 300 µmol, 10 eq.) in DMSO (1 ml).

The dark solid was redispersed in H_2O (10 ml). Diluted NaOH (3 drops) were added to obtain a stable NP solution which was further purified *via* dialysis against demineralised H_2O (in MWCO 12 000, 24 h). The violet, clear NP solution with a particle concentration of 143 nM, was stored at 4 °C in the dark.

TEM: $d = 9.0 \pm 0.9$ nm; UV/Vis: $\lambda_{max} = 526$ nm; DLS: $d_{hydr} = 14 \pm 4$ nm (PDI = 0.08).

Synthesis of Au-MUDA (Ø 10 nm) in H_2O. PPh_3AuCl (16 mg, 31 μmol, 1.0 eq.) in DMSO (3 ml), MUDA (5 mg, 20 μmol, 0.7 eq.) in DMSO (1 ml), t_{Bu}-amine borane (2 mg, 20 μmol, 0.7 eq.) in DMSO (1 ml).

The dark solid was redispersed in H_2O (10 ml). Diluted NaOH (3 drops) were added to obtain a stable NP solution which was further purified *via* dialysis against demineralised H_2O (in MWCO 12 000, 24 h). The violet, clear NP solution with a particle concentration of 115 nM, was stored at 4 °C in the dark.

TEM: $d = 9.7 \pm 0.9$ nm; UV/Vis: $\lambda_{max} = 525$ nm; DLS: $d_{hydr} = 12 \pm 3$ nm (PDI = 0.06).

General synthetic procedure of a ligand exchange reaction

The Au NP solution was filtrated using syringe filtration on a cellulose membrane with 0.2 μm pore size. Then, the NP solution was degassed with argon for 45–90 min. The ligand (as a solid or dissolved) was added dropwise. The pH value of the NP solution was adjusted by the addition of base to achieve a stable clear solution which was stirred at room temperature for a certain time under argon before purification *via* dialysis took place.

Synthesis of Au-MUDA-ADR (Ø 10 nm) in H_2O. Au-MUDA NPs with Ø 10 nm (5 ml) diluted in demineralised H_2O (5 ml), MUDA-ADR (30 mg, 78 μmol) in DMSO (0.5 ml), NEt_3 (3 drops).

The nanoparticle solution was stirred at room temperature for 16 h and directly purified *via* dialysis against demineralised H_2O (in MWCO 12 000, 15 × 2 h). A violet, clear NP solution with a concentration of 101 nM was obtained and stored at 4 °C in the dark.

^{1}H-NMR (600 MHz, D_2O): δ/ppm = 6.81 (s, 1H, C*H*), 6.77–6.69 (m, 1H, C*H*), 6.58–6.51 (m, 1H, C*H*), 4.72–4.66 (m, 1H, C*H*), 2.92–2.82 (m, 3H, CH_3), 2.70–2.63 (m, 2H, CH_2), 2.26–2.10 (m, 2H, CH_2), 1.58–1.46 (m, 4H, CH_2), 1.42–1.35 (m, 2H, CH_2), 1.34–1.20 (m, 12H, CH_2); IR (ATR): ν/cm^{-1} = 3334 (ν_{N-H}, ν_{O-H}), 2921 (ν_{C-H}), 2839, 1691 ($\nu_{C=O}$), 1615 (δ_{N-H}), 1540 (ν_{C-H} + δ_{C-N-H}), 1457 ($\nu_{C=C}$), 1406 (δ_{C-H}), 1368 (δ_{O-H}), 1255 (δ_{C-N}), 1203 (ν_{C-O}), 1128, 1008, 990, 827, 715 (δ_{C-H}), 648 (ν_{C-S}); TEM: $d = 9.9 \pm 0.9$ nm; UV/Vis: $\lambda_{max} = 523$ nm; DLS: $d_{hydr} = 13 \pm 5$ nm (PDI = 0.15).

Synthesis of Au-MUDA-ADR (Ø 9 nm) in H_2O. Au-MUDA NPs with Ø 9 nm (7 ml) diluted in demineralised H_20 (3 ml), MUDA-ADR (15 mg + 10 mg, 65 μmol), triethyl amine (NEt_3) (2 drops).

After degassing of the nanoparticle solution, MUDA-ADR (15 mg in 0.2 ml DMSO) was slowly added and the reaction mixture was stirred at room temperature for 16 h. Further MUDA-ADR (10 mg in 0.2 ml DMSO) was added dropwise and stirred at room temperature for 5 h. Then nanoparticle solution was purified *via* dialysis against demineralised H_2O (in MWCO 12 000, 47 h). A pink, clear NP solution with a concentration of 191 nM was obtained and stored at 4 °C in the dark.

TEM: $d = 8.9 \pm 0.8$ nm; UV/Vis: $\lambda_{max} = 525$ nm; DLS: $d_{hydr} = 13 \pm 3$ nm (PDI = 0.05).

Synthesis of Au-MUDA-ADR (Ø 8 nm) in H_2O. Au-MUDA NPs with Ø 8 nm (5 ml) diluted in demineralised H_2O (5 ml), MUDA-ADR (25 mg, 65 μmol) in DMSO (0.5 ml), NEt_3 (3 drops).

The nanoparticle solution was stirred at room temperature for 16 h and directly purified *via* dialysis against demineralised H_2O (in MWCO 12 000, 6 × 2 h). A violet, clear NP solution with a concentration of 157 nM was obtained and stored at 4 °C in the dark.

TEM: $d = 8.1 \pm 0.6$ nm; UV/Vis: $\lambda_{max} = 526$ nm; DLS: $d_{hydr} = 17 \pm 5$ nm (PDI = 0.09).

Synthesis of Au-MUDA-ADR (Ø 14 nm) in H_2O. Au-citrate NPs with Ø 14 nm (10 ml), MUDA-ADR (20 mg, 52 μmol) in DMSO (0.5 ml), NEt_3 (2 drops).

The nanoparticle solution was stirred at room temperature for 16 h and directly purified *via* dialysis against demineralised H_2O (in MWCO 12 000, 6 × 2 h). A pink, clear NP solution with a concentration of 7.1 nM was obtained and stored at 4 °C in the dark.

TEM: $d = 13.9 \pm 1.2$ nm; UV/Vis: $\lambda_{max} = 525$ nm; DLS: $d_{hydr} = 16 \pm 5$ nm (PDI = 0.10).

Synthesis of Au-MUDA-NA (Ø 10 nm) in H_2O. Au-MUDA NPs with Ø 10 nm (2 ml) were diluted in H_2O (7 ml) and purged with argon for 45 min. MUDA-NA (25 mg, 70 μmol) in DMSO (0.3 ml) was slowly added. Furthermore, NEt_3 (0.1 ml) was added to ensure a stable NP solution which was stirred for 16 h at rt. Then, nanoparticle solution was purified *via* dialysis stepwise against H_2O (in MWCO 12 000, 28 h). A pink, clear NP solution with a concentration of 35 nM was obtained and stored at 4 °C in the dark.

^{1}H NMR (400 MHz, D_2O): δ/ppm = 6.77 (s, 1H, C*H*), 6.72–6.65 (m, 1H, C*H*), 6.58–6.48 (m, 1H, C*H*), 4.60–4.51 (m, 1H, C*H*), 2.58–2.46 (m, 2H, CH_2), 2.24–2.07 (m, 2H, CH_2), 1.74–1.65 (m, 2H, CH_2), 1.58–1.48 (m, 4H, CH_2), 1.38–1.16 (m, 12H, CH_2); IR (ATR): ν/cm^{-1} = 3333 (ν_{O-H}), 2972, 2913 (ν_{C-H}), 2846, 1697 ($\nu_{C=O}$), 1615 (δ_{N-H}), 1571 (ν_{C-H} + δ_{C-N-H}), 1457 ($\nu_{C=C}$), 1376 (δ_{C-H}), 1360 (δ_{O-H}), 1248 (δ_{C-N}), 1165 (ν_{C-O}), 963, 790 (δ_{C-H}), 625 (ν_{C-S}); TEM: $d = 9.9 \pm 0.8$ nm; UV/Vis: $\lambda_{max} = 528$ nm; DLS: $d_{hydr} = 17 \pm 4$ nm (PDI = 0.06).

Animals

Female and male Wistar rats with a body mass of 200–250 g were used for the experiments with colonic mucosa and respiratory smooth muscle. The animals were bred and housed at the Institute for Veterinary Physiology and Biochemistry of the Justus Liebig University Giessen at an ambient temperature of 22.5 °C and air humidity of 50–55% on a 12 h: 12 h light–dark cycle with free access to water and food until the time of the experiment. For the experiments with cardiomyocytes, male rats (175–225 g from Janvier Labs (Le Genest Saint Isles, France)) were housed under similar conditions in the Institute for Physiology. Experiments were approved by the named animal welfare officer of the Justus Liebig University (administrative numbers 561_M and 577_M) performed according to the German and European animal welfare law.

Solutions

The standard solution for the Ussing chamber and the experiments with smooth muscle was a buffer solution containing (mmol l^{-1}): NaCl 107, KCl 4.5, $NaHCO_3$ 25, Na_2HPO_4 1.8,

NaH_2PO_4 0.2, $CaCl_2$ 1.25, $MgSO_4$ 1 and glucose 12. The solution was gassed with carbogen (5% CO_2 in 95% O_2, v/v); pH was 7.4. The experiments with isolated cardiomyocytes were performed in medium 199 with Earle's salts, creatine 5 mmol l^{-1}, L-carnitine 2 mmol l^{-1}, taurine 5 mmol l^{-1}, penicillin 100 U ml^{-1}, and streptomycin 100 μg ml^{-1}.

Tissue preparation

Animal were killed in CO_2 or isoflurane (5% (vol/vol)) narcosis by exsanguination and cervical dislocation. For Ussing chamber experiments, the serosa and tunica muscularis were stripped away by hand to obtain a mucosa-submucosa preparation of the distal colon as described previously.[50] From the trachea, a tube (size 3–4 cartilages) was prepared. In some experiments, a tube from the left primary bronchus (size 6–7 cartilages) was used. Ventricular cardiomyocytes were prepared by collagenase treatment of isolated hearts in a Langendorff perfusion system as previously described.[56]

Short-circuit current measurements

The mucosa-submucosa preparation was fixed in a modified Ussing chamber bathed with a volume of 3.5 ml on each side of the mucosa. The tissue was incubated at 37 °C and short-circuited by a computer-controlled voltage-clamp device (Ingenieur Büro für Mess-und Datentechnik Mussler, Aachen, Germany) with correction for solution resistance. Short-circuit current (I_{sc}) was continuously recorded on a chart-recorder. I_{sc} is expressed as μEq h^{-1} cm^{-2}, *i.e.* the flux of a monovalent ion per time and area, with 1 μEq h^{-1} cm^{-2} = 26.9 μA cm^{-2}. Tissue conductance (G_t; in mS cm^{-2}) was measured every minute by the voltage deviation induced by a current pulse (±50 μA, duration 200 ms) under open-circuit conditions.

Isometric force measurements at smooth muscle from the upper respiratory tract

Force generated by the isolated rings prepared from the upper respiratory tract was measured in an organ bath under isometric conditions. The pretension was set at 2 g. After an equilibrium period of at least 15 min, the tension was lowered to 1 g. As viability control, 30 mmol l^{-1} KCl was administered at the end of each experiment. Isometric force was measured *via* a BioAmp-04/8 amplifier system and sampled *via* an A/D-converter with a sampling rate of 1 Hz (Föhr Medical Instruments, Seeheim, Germany).

Contractility studies at isolated cardiomyocytes

Cells were stimulated at room temperature *via* two AgCl electrodes with biphasic electrical stimuli (amplitude 50 V, duration 5 ms). Cells were stimulated at a frequency of 2 Hz. Every 15 s contractions were recorded. The mean of these four measurements was used to define the cell shortening of a given cell. Cell lengths were measured *via* a line camera (data recording at 500 Hz). Data are expressed as cell shortening normalized to diastolic cell length (dL/L (%)). In each experimental series, randomly selected culture dishes were used to measure dL/L either under control conditions, or in the presence of isoprenaline as positive control, or in the presence of the drugs to be tested.

Drugs

Atenolol, Au-MUDA-ADR, carbachol, ICI-118551 (Tocris, Bristol, UK) and isoprenaline were dissolved in aqueous stock solutions. Bupranolol was dissolved in ethanol (final concentration 0.1% (v/v)). If not indicated otherwise, drugs were from Sigma (Steinheim, Germany).

Statistics

Results are given as mean ± standard error of the mean (SEM) with the number (n) of investigated tissues. For the comparison of two groups either Student's t-test or Mann–Whitney U test was applied. An F-test decided which test method had to be used. Both paired and unpaired two-tailed Student's t-tests were applied as appropriate. When more than two groups had to be compared, an analysis of variances (ANOVA) was performed. If a F-test indicated that variances between the groups were significantly larger than within the groups, a Fishers Least Significant Difference (LSD) *post hoc* test was performed. $P < 0.05$ was considered to be statistically significant.

Author contributions

AM, AW and RC performed experiments. All authors contributed to planning of the experiments, analysis of data and discussion of the results.

Conflicts of interest

There are no conflicts to declare.

Acknowledgements

AM thanks Dr Markus Zegke for scientific input. Furthermore, AM acknowledges Katharina Lauchner for resynthesising ligands and nanoparticles during her project.

References

1 K. Attafi, A. Nattestad, H. Qutaish, M.-S. Park, L. K. Shrestha, K. Ariga, S. X. Dou and J. H. Kim, Solvothermally-synthesized anatase TiO_2 nanoparticles for photoanodes in dye-sensitized solar cells, *Sci. Technol. Adv. Mater.*, 2021, **22**, 100–112.

2 T. Mitsudome, T. Urayama, S. Fujita, Z. Maeno, T. Mizugaki, K. Jitsukawa and K. Kaneda, A Titanium Dioxide Supported Gold Nanoparticle Catalyst for the Selective N-Formylation of Functionalized Amines with Carbon Dioxide and Hydrogen, *ChemCatChem*, 2017, **9**, 3632–3636.

3 S. Azlin-Hasim, M. C. Cruz-Romero, E. Cummins, J. P. Kerry and M. A. Morris, The potential use of a layer-by-layer strategy to develop LDPE antimicrobial films coated with

silver nanoparticles for packaging applications, *J. Colloid Interface Sci.*, 2016, **461**, 239–248.
4 I. Perçin, N. Idil, M. Bakhshpour, E. Yılmaz, B. Mattiasson and A. Denizli, Microcontact Imprinted Plasmonic Nanosensors: Powerful Tools in the Detection of Salmonella paratyphi, *Sensors*, 2017, **17**, 1375.
5 J. N. Anker, W. Paige Hall, O. Lyandres, N. C. Shah, J. Zhao and R. P. Van Duyne, Biosensing with plasmonic nanosensors, *Nat. Mater.*, 2008, 442–453.
6 A. K. Khan, R. Rashid, G. Murtaza and A. Zahra, Gold Nanoparticles: Synthesis and Applications in Drug Delivery, *Trop. J. Pharm. Res.*, 2014, **13**, 1169.
7 L. León Félix, B. Sanz, V. Sebastián, T. E. Torres, M. H. Sousa, J. A. H. Coaquira, M. R. Ibarra and G. F. Goya, Gold-decorated magnetic nanoparticles design for hyperthermia applications and as a potential platform for their surface-functionalization, *Sci. Rep.*, 2019, **9**, 4185.
8 P. Purohit, A. Samadi, P. M. Bendix, J. J. Laserna and L. B. Oddershede, Optical trapping reveals differences in dielectric and optical properties of copper nanoparticles compared to their oxides and ferrites, *Sci. Rep.*, 2020, **10**, 1198.
9 M. C. Arno, M. Inam, A. C. Weems, Z. Li, A. L. A. Binch, C. I. Platt, S. M. Richardson, J. A. Hoyland, A. P. Dove and R. K. O'Reilly, Exploiting the role of nanoparticle shape in enhancing hydrogel adhesive and mechanical properties, *Nat. Commun.*, 2020, **11**, 1420.
10 M. Haruta, N. Yamada, T. Kobayashi and S. Iijima, Gold Catalysts Prepared by Coprecipitation Oxidation for Low-Temperature of Hydrogen and of Carbon Monoxide, *J. Catal.*, 1989, **115**, 301–309.
11 G. Bond and P. A. Sermon, Gold catalysts for olefin hydrogenation, *Gold Bull.*, 1973, **6**, 102–105.
12 G. Bond and D. Thompson, Formulation of mechanisms for gold-catalysed reactions, *Gold Bull.*, 2009, **42**, 247–259.
13 L. Prati, A. Villa, A. Jouve, A. Beck, C. Evangelisti and A. Savara, Gold as a modifier of metal nanoparticles: effect on structure and catalysis, *Faraday Discuss.*, 2018, **208**, 395–407.
14 T. Teranishi, Fabrication and electronic properties of gold nanoparticle superlattices, *C. R. Chim.*, 2003, **6**, 979–987.
15 D. Huang, F. Liao, S. Molesa, D. Redinger and V. Subramanian, Plastic-Compatible Low Resistance Printable Gold Nanoparticle Conductors for Flexible Electronics, *J. Electrochem. Soc.*, 2003, **150**, G412.
16 G. Hajisalem, M. S. Nezami and R. Gordon, Switchable Metal-Insulator Phase Transition Metamaterials, *Nano Lett.*, 2017, **17**, 2940–2944.
17 Y. Zhao, Y. Huang, H. Zhu, Q. Zhu and Y. Xia, Three-in-One: Sensing, Self-Assembly, and Cascade Catalysis of Cyclodextrin Modified Gold Nanoparticles, *J. Am. Chem. Soc.*, 2016, **138**, 16645–16654.
18 M. Khavani, M. Izadyar and M. R. Housaindokht, Theoretical design and experimental study on the gold nanoparticles based colorimetric aptasensors for detection of neomycin B, *Sensor. Actuator. B Chem.*, 2019, **300**, 126947.
19 M. Khavani, M. Izadyar and M. R. Housaindokht, MD/QM modeling of the modified gold nanoparticles and investigation of their sensing ability for selective detection of melamine, *J. Mol. Liq.*, 2019, **284**, 454–461.
20 M. Khavani, M. Izadyar and M. R. Housaindokht, Modeling of the Functionalized Gold Nanoparticle Aggregation in the Presence of Dopamine: A Joint MD/QM Study, *J. Phys. Chem. C*, 2018, **122**, 26130–26141.
21 N. Perets, O. Betzer, R. Shapira, S. Brenstein, A. Angel, T. Sadan, U. Ashery, R. Popovtzer and D. Offen, Golden Exosomes Selectively Target Brain Pathologies in Neurodegenerative and Neurodevelopmental Disorders, *Nano Lett.*, 2019, **19**, 3422–3431.
22 R. Meir, K. Shamalov, T. Sadan, M. Motiei, G. Yaari, C. J. Cohen and R. Popovtzer, Fast Image-Guided Stratification Using Anti-Programmed Death Ligand 1 Gold Nanoparticles for Cancer Immunotherapy, *ACS Nano*, 2017, **11**, 11127–11134.
23 M. Ya Spivak, R. V. Bubnov, I. M. Yemets, L. M. Lazarenko, N. O. Tymoshok and Z. R. Ulberg, Development and Testing of Gold Nanoparticles for Drug Delivery and Treatment of Heart Failure: a Theranostic Potential for PPP Cardiology, *EPMA J.*, 2013, **4**, 20.
24 R. Deng, N. Shen, Y. Yang, H. Yu, S. Xu, Y.-W. Yang, S. Liu, K. Meguellati and F. Yan, Targeting epigenetic pathway with gold nanoparticles for acute myeloid leukemia therapy, *Biomaterials*, 2018, **167**, 80–90.
25 P. Manivasagan, S. Bharathiraja, N. Q. Bui, B. Jang, Y.-O. Oh, I. G. Lim and J. Oh, Doxorubicin-loaded fucoidan capped gold nanoparticles for drug delivery and photoacoustic imaging, *Int. J. Biol. Macromol.*, 2016, **91**, 578–588.
26 M. Camerin, M. Moreno, M. J. Marín, C. L. Schofield, I. Chambrier, M. J. Cook, O. Coppellotti, G. Jori and D. A. Russell, Delivery of a hydrophobic phthalocyanine photosensitizer using PEGylated gold nanoparticle conjugates for the in vivo photodynamic therapy of amelanotic melanoma, *Photochem. Photobiol. Sci.*, 2016, **15**, 618–625.
27 Y. Cheng, A. C Samia, J. D. Meyers, I. Panagopoulos, B. Fei and C. Burda, Highly efficient drug delivery with gold nanoparticle vectors for in vivo photodynamic therapy of cancer, *J. Am. Chem. Soc.*, 2008, **130**, 10643–10647.
28 N. Nagatani, R. Tanaka, T. Yuhi, T. Endo, K. Kerman, Y. Takamura and E. Tamiya, Gold nanoparticle-based novel enhancement method for the development of highly sensitive immunochromatographic test strips, *Sci. Technol. Adv. Mater.*, 2006, **7**, 270–275.
29 N. Mustafaoglu, T. Kiziltepe and B. Bilgicer, Site-specific conjugation of an antibody on a gold nanoparticle surface for one-step diagnosis of prostate specific antigen with dynamic light scattering, *Nanoscale*, 2017, **9**, 8684–8694.
30 A. L. Tomás, M. P. de Almeida, F. Cardoso, M. Pinto, E. Pereira, R. Franco and O. Matos, Development of a Gold Nanoparticle-Based Lateral-Flow Immunoassay for Pneumocystis Pneumonia Serological Diagnosis at Point-of-Care, *Front. Microbiol.*, 2019, **10**, 2917.

31 N. A. Byzova, I. V. Safenkova, E. S. Slutskaya, A. V. Zherdev and B. B. Dzantiev, Less is More: A Comparison of Antibody-Gold Nanoparticle Conjugates of Different Ratios, *Bioconjugate Chem.*, 2017, **28**, 2737–2746.
32 J. Polte, R. Erler, A. F. Thünemann, S. Sokolov, T. T. Ahner, K. Rademann, F. Emmerling and R. Kraehnert, Nucleation and growth of gold nanoparticles studied via in situ small angle X-ray scattering at millisecond time resolution, *ACS Nano*, 2010, **4**, 1076–1082.
33 R. Arvizo, R. Bhattacharya and P. Mukherjee, Gold nanoparticles: opportunities and challenges in nanomedicine, *Expet Opin. Drug Deliv.*, 2010, **7**, 753–763.
34 B. Fortuni, T. Inose, M. Ricci, Y. Fujita, I. van Zundert, A. Masuhara, E. Fron, H. Mizuno, L. Latterini, S. Rocha and H. Uji-I, Polymeric Engineering of Nanoparticles for Highly Efficient Multifunctional Drug Delivery Systems, *Sci. Rep.*, 2019, **9**, 2666.
35 A. Mattern, F. Machka, M. S. Wickleder, O. S. Ilyaskina, M. Bünemann, M. Diener and E. Pouokam, Potentiation of the activation of cholinergic receptors by multivalent presentation of ligands supported on gold nanoparticles, *Org. Biomol. Chem.*, 2018, **16**, 6680–6687.
36 F. Gasiorek, E. Pouokam, M. Diener, S. Schlecht and M. S. Wickleder, Effects of multivalent histamine supported on gold nanoparticles: activation of histamine receptors by derivatized histamine at subnanomolar concentrations, *Org. Biomol. Chem.*, 2015, **13**, 9984–9992.
37 S. Liese and R. R. Netz, Quantitative Prediction of Multivalent Ligand-Receptor Binding Affinities for Influenza, Cholera, and Anthrax Inhibition, *ACS Nano*, 2018, **12**, 4140–4147.
38 Y. Zhang, M. Cheng, J. Cao, Y. Zhang, Z. Yuan, Q. Wu and W. Wang, Multivalent nanoparticles for personalized theranostics based on tumor receptor distribution behavior, *Nanoscale*, 2019, **11**, 5005–5013.
39 R. Riessen, O. Tschritter, U. Janssens and M. Haap, Katecholamine: Pro und Kontra, *Med. Klin. Intensivmed. Notfallmed.*, 2016, **111**, 37–46.
40 M. Johnson, Beta2-adrenoceptors: mechanisms of action of beta2-agonists, *Paediatr. Respir. Rev.*, 2001, **2**, 57–62.
41 G. P. Maier, C. M. Bernt and A. Butler, Catechol oxidation: considerations in the design of wet adhesive materials, *Biomater. Sci.*, 2018, **6**, 332–339.
42 E. A. Pillar, R. C. Camm and M. I. Guzman, Catechol oxidation by ozone and hydroxyl radicals at the air-water interface, *Environ. Sci. Technol.*, 2014, **48**, 14352–14360.
43 O. Abed, M. Wanunu, A. Vaskevich, R. Arad-Yellin, A. Shanzer and I. Rubinstein, Reversible Binding of Gold Nanoparticles to Polymeric Solid Supports, *Chem. Mater.*, 2006, **18**, 1247–1260.
44 D. G. Brown and J. Boström, Analysis of Past and Present Synthetic Methodologies on Medicinal Chemistry: Where Have All the New Reactions Gone?, *J. Med. Chem.*, 2016, **59**, 4443–4458.
45 E. Oh, K. Susumu, J. B. Blanco-Canosa, I. L. Medintz, P. E. Dawson and H. Mattoussi, Preparation of stable maleimide-functionalized au nanoparticles and their use in counting surface ligands, *Small*, 2010, **6**, 1273–1278.
46 G. Frens, Controlled Nucleation for the Regulation of the Particle Size in Monodisperse Gold Suspensions, *Nat. Phys. Sci.*, 1973, 20–22.
47 S. K. Sivaraman, S. Kumar and V. Santhanam, Monodisperse sub-10 nm gold nanoparticles by reversing the order of addition in Turkevich method – the role of chloroauric acid, *J. Colloid Interface Sci.*, 2011, **361**, 543–547.
48 N. Zheng, J. Fan and G. D. Stucky, One-step one-phase synthesis of monodisperse noble-metallic nanoparticles and their colloidal crystals, *J. Am. Chem. Soc.*, 2006, **128**, 6550–6551.
49 P. Pengo, S. Polizzi, M. Battagliarin, L. Pasquato and P. Scrimin, Synthesis, characterization and properties of water-soluble gold nanoparticles with tunable core size, *J. Mater. Chem.*, 2003, **13**, 2471–2478.
50 S. Hörger, G. Schultheiß and M. Diener, Segment-specific effects of epinephrine on ion transport in the colon of the rat, *Am. J. Physiol.*, 1998, **275**, G1367–G1376.
51 J. Zhang, S. T. Halm and D. R. Halm, Adrenergic activation of electrogenic K+ secretion in guinea pig distal colonic epithelium: involvement of beta1- and beta2-adrenergic receptors, *Am. J. Physiol. Gastrointest. Liver Physiol.*, 2009, **297**, G269–G277.
52 M. Patel and D. Shaw, A review of standard pharmacological therapy for adult asthma – Steps 1 to 5, *Chron. Respir. Dis.*, 2015, **12**, 165–176.
53 C. Jenkins, A. B. X. Breslin and G. E. Marlin, The role of alpha and beta adrenoceptors in airway hyperresponsiveness to histamine, *J. Allergy Clin. Immunol.*, 1985, 364–372.
54 X. Xu, J. Kaindl, M. J. Clark, H. Hübner, K. Hirata, R. K. Sunahara, P. Gmeiner, B. K. Kobilka and X. Liu, Binding pathway determines norepinephrine selectivity for the human β1AR over β2AR, *Cell Res.*, 2021, **31**, 569–579.
55 E. C. Hulme and M. A. Trevethick, Ligand binding assays at equilibrium: validation and interpretation, *Br. J. Pharmacol.*, 2021, 1219–1237.
56 F. Nippert, R. Schreckenberg and K.-D. Schlüter, Isolation and Cultivation of Adult Rat Cardiomyocytes, *JoVE*, 2017, DOI: 10.3791/56634.